The Astrophysical Journal Letters, 868:L18 (5pp), 2018 December 1 https://doi.org/10.3847/2041-8213/aaef3a

Energy Partition between Ion and Electron of Collisionless Magnetic Reconnection

Masahiro Hoshino
Department of Earth and Planetary Science, The University of Tokyo, Tokyo 113-0033, Japan; hoshino@eps.s.u-tokyo.ac.jp
Received 2018 October 11; revised 2018 November 6; accepted 2018 November 7; published 2018 November 20

Abstract

The plasma heating during collisionless magnetic reconnection is investigated using particle-in-cell simulations. We analyze the time evolution of the plasma temperature associated with the motion of the reconnecting flux tube, where the plasma temperature is defined as the second-order moment of the velocity distribution function in the simulation frame/in the center of the flux tube frame, and we show that the plasma heating during magnetic reconnection can be separated into two distinct stages: the nonadiabatic heating stage, in which the magnetic field lines are just reconnecting in the X-type diffusion region, and the adiabatic heating stage, in which the flux tube is shrinking after two flux tubes merge. During the adiabatic heating stage, the plasma temperature T can be approximated by $TV^{\gamma-1} = \text{const.}$, where $\gamma = 5/3$ is the specific heat, and V is the volume of the flux tube. In the nonadiabatic heating stage, we found numerically that the ratio of the increment of the ion temperature to that of the electron temperature can be approximated by $\Delta T_i/\Delta T_e \approx (m_i/m_e)^{1/4}$, where m_i and m_e are the ion and electron masses, respectively. We also present a theoretical model based on a magnetic-diffusion-dominated reconnection to explain the simulation result.

Key words: magnetic reconnection – plasmas

1. Introduction

High-energy astrophysical phenomena such as planetary magnetospheres, solar flares, pulsar wind nebulae, astrophysical jets and magnetars often contain the high magnetic energy density that exceeds the plasma energy density (e.g., Lyubarsky & Kirk 2001; Spruit 2010; Uzdensky 2011; Cerutti et al. 2013; Sironi & Spitkovsky 2014). By releasing the magnetic field energy into energetic particles and electromagnetic radiations, dramatic magnetoactive phenomena can be observed (e.g., Birn et al. 2012; Hoshino & Lyubarsky 2012; Blandford et al. 2017). While magnetic reconnection is believed to be the major energy conversion process in these sources, energy partition between hadronic and leptonic components during reconnection remains a fundamental quest in hot and dilute collisionless plasma. Nonequipartition of energy between ion and electron is often a key issue to discuss the dynamical evolution of the astrophysical phenomena. We discuss the energy partition during collisionless magnetic reconnection.

It is observationally known that ions are preferentially heated compared to electrons during magnetic reconnection in the earth's magnetotail, and that the ion temperature is several times greater than the electron one (Baumjohann et al. 1989; Wang et al. 2012; Eastwood et al. 2013). Conversion of energy into plasma heat has also been observationally investigated in other types of reconnection in the solar wind and at the earth's magnetopause, and it is found that the energy transfer to ions is larger than that to electrons (Phan et al. 2013). In addition to space observations, kinetic simulations using the particle-in-cell (PIC) method also suggest that the energy gain of ions is larger than that of electrons, and that energy transfer to ions can increase as the mass ratio of ions to electrons increases (e.g., Shay et al. 2014; Haggerty et al. 2015). The mechanism of energy conversion from stored magnetic energy into ion and electron heating is a principal topic of reconnection, but the energy partition remains under debate.

One of the difficulties in understanding the energy partition during reconnection is that the ion and electron temperatures are not uniform in space and time. Plasmas are quickly heated when the upstream plasma initially enters the magnetic diffusion region located at the X-type point, and some of the accelerated high-energy particles are ejected outward along the magnetic field lines (e.g., Decoster & Frank 1979; Birn et al. 2012; Egedal et al. 2013); their free energies, stored in the form of beams, are then released in the separatrix away from the X-type point (e.g., Hesse et al. 2001; Hoshino et al. 2001; Birn et al. 2012). In addition, the magnetic field lines reconnected at the diffusion region are transported downstream into the reconnection exhaust (e.g., Hoshino et al. 1998; Lottermoser et al. 1998; Drake et al. 2009) and the plasma temperatures increase further owing to plasma compression (e.g., Imada et al. 2005).

To date, the plasma heating process and its energy partition mechanism have been discussed by comparing the temperatures upstream of the reconnection region with those of the downstream/exhaust region (Eastwood et al. 2013; Phan et al. 2013; Shay et al. 2014, 2018; Haggerty et al. 2015). In this Letter, however, we analyze the plasma temperature associated with the motion of the reconnecting magnetic flux tube in order to distinguish the adiabatic and nonadiabatic heating processes. If no energy dissipation due to the nonadiabatic process exists, the plasma entropy p/ρ^{γ} along the plasma flow, i.e., along the so-called Lagrangian plasma flow, should be conserved.

It is usually not easy to analyze the evolution of the gas pressure and density in Lagrangian flow, but under the frozen-in condition between magnetic field lines and plasmas, Lagrangian flow can coincide with the motion of the magnetic field lines outside of the diffusion region, and the motion of the magnetic field can be easily described using the contour of the vector potential in a two-dimensional system in space. Using this simple idea, we define the flux tube volume and plasma temperature integrated over the magnetic flux tube, and we show that the time evolution of the ion and electron

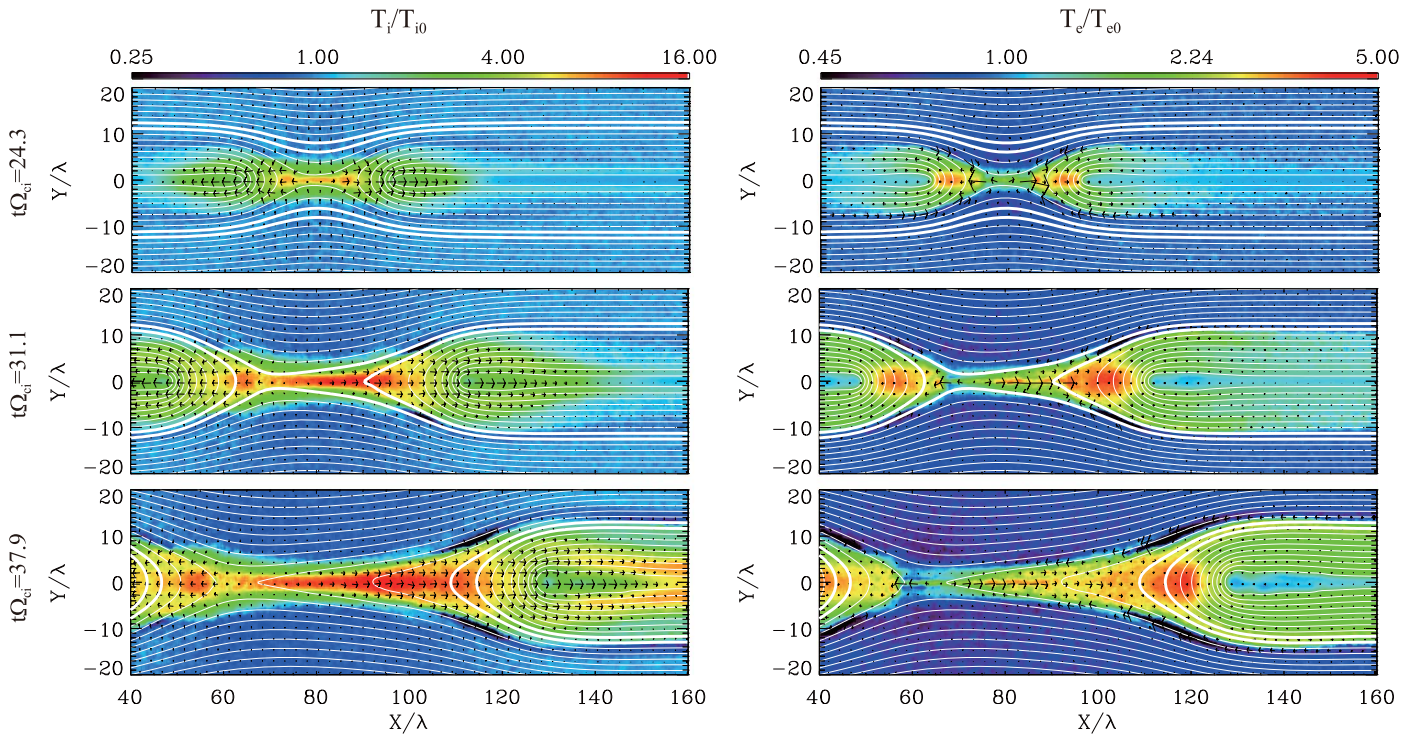

Figure 1. Time evolution of collisionless magnetic reconnection. Left and right panels show the ion and electron temperatures, respectively. The white lines represent magnetic field lines, and the thick white lines show a typical magnetic flux tube moving with the plasma flow. Black arrows indicate the flow vectors in arbitrary units. Top to bottom: the stage before two flux tubes are reconnected, the reconnection stage, and the stage after two flux tubes merge.

temperatures can be separated into two processes: effective ohmic heating in the diffusion region and an adiabatic compression process associated with the outward plasma convection in the reconnection exhaust.

2. Thermodynamical Properties of the Magnetic Flux Tube

Figure 1 shows the time evolution of magnetic reconnection obtained by a two-dimensional PIC simulation with a periodic boundary in the x direction and conducting walls for the upper and lower boundaries at $y = \pm 40\lambda$, where λ is the thickness of the initial plasma sheet. The total system size is $160\lambda \times 80\lambda$, and the grid size is 6400×3200. Part of the simulation domain is depicted. The spatial scale is normalized by the thickness of the plasma sheet λ. The mass ratio of ions to electrons is $m_i/m_e = 400$, and Harris equilibrium with the same ion and electron temperature $T_{i0} = T_{e0}$ is assumed. The total number of particles is 2.2×10^{10}, i.e., 538×2 particles/grid cell in order to calculate the high β plasma sheet as accurately as possible. The ion and electron inertial lengths are $V_A/\Omega_{ci} = 56.5$ and $c/\Omega_{pe} = 2.8$ grid points, respectively, and λ has 40 grid points. The ion drift velocity is set to be the same as the ion thermal velocity. The background plasma density in the upstream region is 5% of the maximum density of the plasma sheet.

The color contour in Figure 1 shows the ion and electron temperatures normalized by the initial temperature, and the scales are indicated by the bars at the top of the panels. The white lines are the magnetic field lines calculated from the contour of the vector potential $A_z(x, y, t)$, and the thick white lines show the time evolution of the flux tube. We observe that the flux tube is transported from the upstream region to the reconnection exhaust during plasma convection. Note that if the frozen-in flux condition between the plasma and magnetic field is satisfied, the condition of $\boldsymbol{E} + \boldsymbol{v} \times \boldsymbol{B}/c = 0$ is equivalent to the equation $(\partial/\partial t + \boldsymbol{v} \cdot \nabla)A_z = 0$ in the two-dimensional system. Then the plasma quantities associated with the plasma flow motion as Lagrangian flow motion can be determined from the contour of the vector potential A_z.

Two flux tubes at $t\Omega_{ci} = 24.3$ are located in the upstream region and are not yet reconnected. The ion and electron temperatures remain low. At $t\Omega_{ci} = 31.1$, the flux tubes are just reconnecting, and they surround both the X-type diffusion region and the boundary region of the magnetic separatrix. Both ions and electrons are heated in the diffusion region, and the hot plasma is ejected outward. At $t\Omega_{ci} = 37.9$, outside the margin of the two flux tubes, the closed flux tube starts to shrink and surrounds the O-type point. The plasma in the shrinking flux tube is compressed, and its temperature increases further. This time evolution is the same as that observed in other PIC simulations performed by many researchers to date (e.g., Hoshino et al. 1998).

Figure 2(a) shows the time evolution of the total particle number of ions (red circles) and electrons (blue squares) in the flux tube in Figure 1. The number is normalized by the average number during reconnection. We can see that the particle numbers for ions and electrons are almost conserved within an error of approximately 1%, and we find that the frozen-in condition between the plasma and magnetic field lines is almost satisfied. However, as we expected, a slightly large departure appears in the stage where $t\Omega_{ci} = 27$–33, which corresponds to slippage of the magnetic field lines during the passage of the flux tube through the diffusion region. We can also observe that the slippage of ions, which have larger gyroradii, is slightly larger than that of electrons. The frozen-in condition of the plasma and magnetic field lines is not perfectly satisfied, but roughly speaking, both ions and electrons are moving together with the motion of the flux tube, probably because the effective

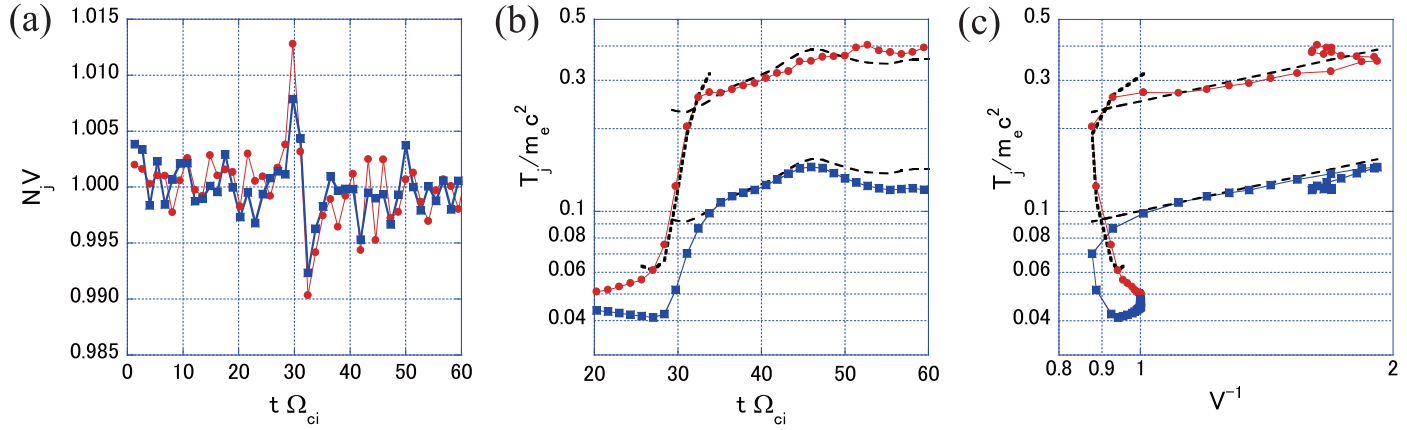

Figure 2. (a) Time history of the total particle numbers of ions (red circles) and electrons (blue squares) integrated over the volume of the magnetic flux tube shown in Figure 1. (b) Time history of ion (red) and electron (blue) temperatures. The temperatures are normalized by the electron rest mass energy. The dashed lines after $t\Omega_{ci} = 32$ are the adiabatic relation with $T_j V^{2/3} = \text{const.}$, and the dotted line between $27 < t\Omega_{ci} < 32$ is obtained using the effective ohmic heating model. (c) Phase diagram for the reciprocal of the flux volume and the temperatures for ions (red) and electrons (blue). The dashed and dotted lines have the same meaning as those in (b).

magnetic Reynolds number is large in collisionless reconnection. From this result, we can use the motion of the magnetic flux tube as a tracer of the Lagrangian plasma flow.

Figure 2(b) shows the time history of the ion and electron temperatures averaged over the flux tube shown in Figure 1. The temperature is calculated by taking the second-order moment of the velocity distribution function in the simulation frame (i.e., in the center of the flux tube frame), and our temperature includes the bulk flow energy, because we study the gross kinetic energy contained inside the flux tube. Figure 2(c) is a phase diagram of the relationship between their temperatures and the volume of the flux tube V, which is defined as the area sandwiched between the magnetic field lines. Because the ion and electron particle numbers in the flux tube are unchanged from those in Figure 2(a), taking the reciprocal of the volume, V^{-1} yields the averaged plasma density for the flux tube. We normalized the volume of the flux tube by that in the initial state.

In the initial state of $t\Omega_{ci} = 0$ in Figure 2(c), both ions and electrons are situated at $(T, V^{-1}) = (0.05,1)$, and the flux tube is located outside the plasma sheet. With increasing time, but still in the early stage ($t\Omega_{ci} < 27$) in Figures 2(b) and (c), both the ions and electrons remain cold, but the electrons are slightly cooler, probably because of adiabatic expansion of the magnetized electrons. As the flux tube is convected toward the plasma sheet, the outward-propagating slow expansion wave from the X-point causes the flux tube to widen (see the widening of the flux tube above and below the X-type point at $t\Omega_{ci} = 24.3$ in Figure 1).

When the flux tube is crossing the diffusion region at $t\Omega_{ci} = 27$–33, which is the time at which the flux tube exhibits slippage in Figure 2(a), both the ion and electron temperatures start to increase rapidly. The electron temperature doubles, whereas the ion temperature becomes almost four times larger. From Figure 2(c), we find that the volume of the flux tube does not change very much. The increase in plasma temperature is independent of the flux tube compression, suggesting that the energy gain originated in a nonadiabatic process, probably effective ohmic heating by collisionless inertial resistivity.

For $t\Omega_{ci} > 35$, i.e., after the flux tube has finished crossing the diffusion region, both ions and electrons are gradually heated as the flux tube is transported outward. We found that the gradual increases in the temperatures T_i and T_e are almost proportional to $1/V^{\gamma-1}$ with $\gamma = 5/3$, as denoted by the black dashed lines in Figures 2(b) and (c). This suggests that the adiabatic heating process dominates both ions and electrons after the two flux tubes merge. Although the plasma temperature inside the flux tube is not uniform in space, it is interesting to note that the temperature averaged over the flux tube satisfies the relation describing the adiabatic process.

At a later time stage, we can see that the temperature oscillates. Owing to the periodic boundary in x, the high-pressure plasmoid in and around the O-type point pushes the reconnection outflow backward, and compression and expansion of the high-pressure plasmoid can be seen. From Figures 2(b) and (c), we may conclude that the reconnection heating can be clearly separated into two stages, the nonadiabatic process during the magnetic field reconnection stage and the adiabatic process after reconnection. Note that during the adiabatic process, the ratio of the ion temperature to the electron temperature does not change, and thus the final energy partition seems to be determined solely during the nonadiabatic process.

Let us discuss the preferential heating during the nonadiabatic stage. Figure 3(a) shows the relationship between the ion and electron temperatures during magnetic reconnection; we focus on the nonadiabatic process stage for $t\Omega_{ci} = 27.0$–32.4. The increase in the ion temperature is almost proportional to the increase in the electron one, and the red line is a linear fitting line with a slope of 4.31. In addition to analyzing the typical flux tube shown in Figure 1, we performed the same analysis for other magnetic flux tubes in Figure 1 and found that the ratio of the increment of the ion temperature to that of the electron temperature, $\Delta T_i/\Delta T_e$, is approximated by 4.06 ± 0.26.

The energy partition between ions and electrons should depend on the mass ratio of ions to electrons artificially assumed in the PIC simulation. Therefore, in addition to the PIC simulation of the mass ratio $m_i/m_e = 400$ in Figure 1, we performed other simulation runs with $m_i/m_e = 6.25$, 25 and 100. Figure 3(b) shows the dependence of the energy partition on the mass ratio. If we can fit the mass dependence by a power-law function of m_i/m_e, the best fit can be

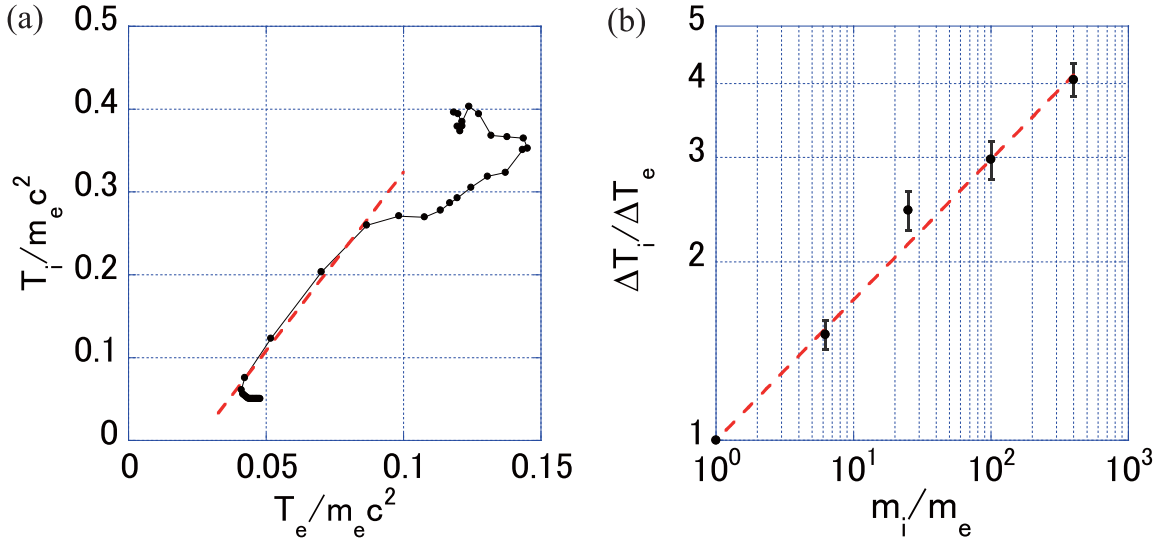

Figure 3. (a) Time history of ion and electron temperatures integrated along the magnetic flux tube. The red line is the best fit for the nonadiabatic heating stage. (b) Mass dependence of the ratio of the increment of the ion temperature to the electron temperature. Red line is the power-law fitting $(m_i/m_e)^p$ with $p = 0.237$.

approximated by

$$\frac{\Delta T_i}{\Delta T_e} = \left(\frac{m_i}{m_e}\right)^{0.237\pm0.005}. \quad (1)$$

Note that we assumed $\Delta T_i/\Delta T_e = 1$ for the pair plasma.

According to this scaling law, we will be able to estimate the increment of the ion temperature for a given electron temperature. The dotted lines in the nonadiabatic stage in Figures 2(b) and (c) are obtained by assuming $\Delta T_i/\Delta T_e = (m_i/m_e)^{1/4} = 4.47$. We find that the dotted lines are almost superposed on the ion temperature curves.

3. Nonadiabatic Heating Process

Let us discuss theoretically the nonadiabatic heating process. We think that there are two important heating processes involved in this stage: one is energy dissipation in the magnetic diffusion region, which is provided by the effective ohmic heating under the collisionless inertial resistivity. The other is kinetic heating in the magnetic separatrix, namely, the boundary between the upstream region of the plasma sheet and the plasma outflow region with reconnection jet flows.

We first estimate the energy gain in the diffusion region. The effective ohmic heating rates Q_j of ions and electrons integrated over the ion/electron diffusion region can be estimated as $Q_j = EJ_jS_j$, where E, J_j, and S_j are the reconnection electric field, ion/electron electric current, and volume of the ion/electron diffusion region, respectively. The volume of the diffusion region in a two-dimensional system, $S_j = \Delta_j d_j$, may be simply assumed to be a rectangular box with Δ_j in the x direction and d_j in the y direction.

In collisionless reconnection, d_j can be easily evaluated using the bounce motion across the neutral sheet, which is the so-called meandering particle orbit, where the local gyroradius becomes comparable to the distance d_j from the X-type neutral point, and Δ_j is the gyroradius of the reconnected magnetic field described by the Speiser orbit. Namely, $d_j = \sqrt{\lambda_y v_{j,\mathrm{in}}/\Omega_{j,\mathrm{in}}}$, and $\Delta_j = \sqrt{\lambda_x v_{j,\mathrm{out}}/\Omega_{j,\mathrm{out}}}$, where λ_x and λ_y are the scale lengths of the magnetic field gradient in the x and y directions, respectively. Furthermore, $v_{j,\mathrm{out}}/\Omega_{j,\mathrm{out}}$ and $v_{j,\mathrm{in}}/\Omega_{j,\mathrm{in}}$ are the gyroradius defined by the outflow/inflow velocity and the gyrofrequency based on the asymptotic magnetic field strength in the outflow/inflow region, respectively (e.g., Coroniti 1985; Büchner & Zelenyi 1989).

The ion/electron electric current inside the diffusion region can be evaluated using Ohm's law, $J_j = \sigma_j E$, where $\sigma_j = ne^2/m_j\nu_j$ is the effective electric conductivity. For collisionless reconnection, the effective collision frequency, $\nu_j = v_{j,\mathrm{out}}/\Delta_j$, can be estimated from the finite residence time in the magnetic diffusion region, because the resonance between the reconnection electric field E and the particle acceleration due to E is the origin of the inertial resistivity in collisionless reconnection (e.g., Coppi et al. 1966; Hoh 1966).

In the inflow region, the plasmas are convected by $E \times B$ drift motion, whose speed is much smaller than the Alfvén speed, defined by the magnetic field in the asymptotic field strength upstream and the plasma density in the plasma sheet. As we assumed that the background plasma temperature upstream is the same as that in the plasma sheet, the Alfvén speed is almost the same as the ion thermal velocity. As long as the ion and electron thermal velocities are larger than $E \times B$ drift velocity, $v_{j,\mathrm{in}}$ for the meandering motion may be estimated to be their thermal velocities of $\sqrt{2T_{j0}/m_j}$, respectively.

Using the above relations, we can obtain,

$$\frac{J_i\Delta_i}{J_e\Delta_e} = \frac{\sigma_i\Delta_i}{\sigma_e\Delta_e} = \left(\frac{m_e v_{e,\mathrm{out}}}{m_i v_{i,\mathrm{out}}}\right) \times \left(\frac{\Delta_i}{\Delta_e}\right)^2 = 1,$$

and

$$\frac{d_i}{d_e} = \left(\frac{v_{i,\mathrm{in}} m_i}{v_{e,\mathrm{in}} m_e}\right)^{1/2} = \left(\frac{m_i T_{i0}}{m_e T_{e0}}\right)^{1/4}.$$

Then the ratio of the effective ohmic heating of ion to electron integrated over the magnetic diffusion region and the ratio of the increment of temperatures averaged over the flux tube are

given by

$$\frac{Q_i}{Q_e} = \frac{\Delta T_i}{\Delta T_e} = \frac{J_i E S_i}{J_e E S_e} = \frac{\sigma_i \Delta_i d_i}{\sigma_e \Delta_e d_e} = \left(\frac{m_i T_{i0}}{m_e T_{e0}}\right)^{1/4}. \quad (2)$$

This result is in good agreement with the numerical simulation result in Equation (1) during the nonadiabatic heating stage.

As one can see by the above theoretical argument, our estimation does not explicitly include the nonadiabatic heating process at the separatrix boundary, but we implicitly took account of the energy gain at the boundary due to the plasma beam population/heat flux emanating from the diffusion region. As long as the distance is not far from the diffusion region, the plasma heating at the separatrix would be provided through the beam plasma instability between the cold component transported by $E \times B$ drift motion from the upstream and the beam component coming from the diffusion region (e.g., Hoshino et al. 1998), and the free energy of the beam plasma instability is mainly carried by the beam component (e.g., Hoshino et al. 1998; Lottermoser et al. 1998).

At the separatrix boundary far from the diffusion region, the contribution from the local plasma heating by the pick-up plasma process across the boundary may dominate, but our simulation size is several times larger as compared to the size of the magnetic diffusion region. In fact, the plasma sheet is known to be unstable to the tearing mode instability (e.g., Coppi et al. 1966; Hoh 1966), and the separation distance between two X-type points may not be large compared to the size of the diffusion region. Sironi & Spitkovsky (2014) show the sporadic formation of many plasmoids in the plasma sheet. For such a plasmoid-dominated reconnection, our theoretical argument based on the magnetic-diffusion-dominated, nonadiabatic heating seems to be valid.

4. Summary and Discussion

We discussed the time evolution of ion and electron temperature integrated along the time evolving magnetic flux tube for a plasma sheet with the antiparallel magnetic field topology, and found that the plasma heating process during reconnection can be separated into two stages of adiabatic and nonadiabatic processes. Except for the time stage of two flux tubes merging, the heating process can be approximated by the adiabatic heating from the macroscopic point of view. We also found in the nonadiabatic heating stage of two flux tubes merging that the increment of ion and electron temperature ratio is proportional to $(m_i/m_e)^{1/4}$.

Our simulation study in the two-dimensional system with the antiparallel magnetic field topology is only a first step toward understanding the energy partition between ion and electron in a variety of astroplasma environments. It is important to further examine our simple model of adiabatic versus nonadiabatic heating in more general cases. For a case of non-anti-parallel magnetic field topology with a finite guide field, the mechanism of the collisionless energy dissipation in the magnetic diffusion region would be different from our theoretical argument in Equation (2) (Drake & Lee 1977). In the three-dimensional system, the lower-hybrid drift instability would also be also expected to contribute to electron heating in the plasma sheet boundary in the three-dimensional system (Davidson & Gladd 1975; Shinohara et al. 2001). Recent three-dimensional PIC simulations with a finite guide field show that the diffusion region becomes a highly dynamical state in association with a spontaneous formation of the flux rope (Daughton et al. 2011; Liu et al. 2013). A study of the plasma heating in a three-dimensional and larger-scale system would be especially important.

In the Letter, we discussed the energy partition between two compositions of ion and electron, but our findings may have important implications for the energy partition of multi-component plasmas, including heavy ions observed in solar flares and in the Earth's substorms.

This work was supported by JSPS Grant-in-Aid for Scientific Research (KAKENHI) grant No. 18K18748. The author thanks T. Amano, W. Baumjohann, J. Büchner, C. C. Haggerty, M. Hesse, H. Ji, R. Nakamura, Y. Ohira, A. Vivads, and L. M. Zelenyi for valuable discussions.

ORCID iDs

Masahiro Hoshino https://orcid.org/0000-0002-1818-9927

References

Baumjohann, W., Paschmann, G., & Cattell, C. A. 1989, JGR, 94, 6597
Birn, J., Artemyev, A. V., Baker, D. N., et al. 2012, SSRv, 173, 49
Blandford, R., Yuan, Y., Hoshino, M., & Sironi, L. 2017, SSRv, 207, 291
Büchner, J., & Zelenyi, L. M. 1989, JGR, 94, 11821
Cerutti, B., Werner, G. R., Uzdensky, D. A., & Begelman, M. C. 2013, ApJ, 770, 147
Coppi, B., Laval, G., & Pellat, R. 1966, PhRvL, 16, 1207
Coroniti, F. V. 1985, JGR, 90, 7427
Daughton, W., Roytershteyn, V., Karimabadi, H., et al. 2011, NatPh, 7, 539
Davidson, R. C., & Gladd, N. T. 1975, PhFl, 18, 1327
Decoster, R. J., & Frank, L. A. 1979, JGR, 84, 5099
Drake, J. F., & Lee, Y. C. 1977, PhFl, 20, 1341
Drake, J. F., Swisdak, M., Phan, T. D., et al. 2009, JGRA, 114, A05111
Eastwood, J. P., Phan, T. D., Drake, J. F., et al. 2013, PhRvL, 110, 225001
Egedal, J., Le, A., & Daughton, W. 2013, PhPl, 20, 061201
Haggerty, C. C., Shay, M. A., Drake, J. F., Phan, T. D., & McHugh, C. T. 2015, GeoRL, 42, 9657
Hesse, M., Birn, J., & Kuznetsova, M. 2001, JGR, 106, 3721
Hoh, F. C. 1966, PhFl, 9, 277
Hoshino, M., & Lyubarsky, Y. 2012, SSRv, 173, 521
Hoshino, M., Mukai, T., Terasawa, T., & Shinohara, I. 2001, JGR, 106, 25979
Hoshino, M., Mukai, T., Yamamoto, T., & Kokubun, S. 1998, JGR, 103, 4509
Imada, S., Hoshino, M., & Mukai, T. 2005, GeoRL, 32, L09101
Liu, Y.-H., Daughton, W., Karimabadi, H., Li, H., & Roytershteyn, V. 2013, PhRvL, 110, 265004
Lottermoser, R.-F., Scholer, M., & Matthews, A. P. 1998, JGR, 103, 4547
Lyubarsky, Y., & Kirk, J. G. 2001, ApJ, 547, 437
Phan, T. D., Shay, M. A., Gosling, J. T., et al. 2013, GeoRL, 40, 4475
Shay, M. A., Haggerty, C. C., Matthaeus, W. H., et al. 2018, PhPl, 25, 012304
Shay, M. A., Haggerty, C. C., Phan, T. D., et al. 2014, PhPl, 21, 122902
Shinohara, I., Suzuki, H., Fujimoto, M., & Hoshino, M. 2001, PhRvL, 87, 095001
Sironi, L., & Spitkovsky, A. 2014, ApJL, 783, L21
Spruit, H. C. 2010, in The Jet Paradigm, Lecture Notes in Physics, Vol. 794, ed. T. Belloni (Berlin: Springer), 233
Uzdensky, D. A. 2011, SSRv, 160, 45
Wang, C.-P., Gkioulidou, M., Lyons, L. R., & Angelopoulos, V. 2012, JGRA, 117, A08215